minerals

MDPI

Article

Improved Quartz Flotation at Low Temperature by Amino Acid Lauryl Lysine as a Novel Green Collector

Fei Wu [1,2], Shaohang Cao [1,2,3,*], Wanzhong Yin [4], Yafeng Fu [5], Chao Li [1,2,3] and Yijun Cao [1,2,3,*]

1 Zhongyuan Critical Metals Laboratory, Zhengzhou University, Zhengzhou 450001, China; wf15286881721@gs.zzu.edu.cn (F.W.); c.li@zzu.edu.cn (C.L.)
2 School of Chemical Engineering, Zhengzhou University, Zhengzhou 450001, China
3 The Key Lab of Critical Metals Minerals Supernormal Enrichment and Extraction, Ministry of Education, Zhengzhou 450001, China
4 School of Resources and Civil Engineering, Northeastern University, Shenyang 110819, China; yinwanzhong@mail.neu.edu.cn
5 Ansteel Beijing Research Institute Co., Ltd., Beijing 102200, China; fuyafeng110@126.com
* Correspondence: sh_cao@zzu.edu.cn (S.C.); yijuncao@zzu.edu.cn (Y.C.)

Abstract: A new type of amino acid surfactant, lauroyl lysine (LL), is used as a green collector for the low-temperature flotation of quartz. The micro-flotation test results indicate that, under flotation conditions of 10–40 °C, pH = 11.0, 20 mg/L $CaCl_2$, and 60 mg/L LL, the highest recovery of quartz by LL could reach up to 97.08%. The temperature at which flotation occurs little impacts LL collection efficiency. In contrast, sodium oleate (NaOL) gives inferior performance to LL at all tested temperatures. The adsorption measurement and SEM-EDS results confirm that a quantity of LL is absorbed onto the quartz surface at low temperatures. Investigations into the interaction between the reagents and mineral surfaces are conducted using X-ray photoelectron spectroscopy (XPS) analysis, zeta potential measurements, and Fourier transform infrared (FT-IR) spectra. Findings indicate that LL is adsorbed onto the quartz surface through hydrogen bonds and intense chemisorption. Additionally, the amide groups in the LL molecular structure increase the solubility of the collector at low temperatures, and simultaneously, the amide bond can form an intermolecular hydrogen bond between O and H, which is conducive to quartz flotation.

Keywords: amino acid; flotation; low temperature; green collector; quartz; lauroyl lysine

check for updates

Citation: Wu, F.; Cao, S.; Yin, W.; Fu, Y.; Li, C.; Cao, Y. Improved Quartz Flotation at Low Temperature by Amino Acid Lauryl Lysine as a Novel Green Collector. *Minerals* **2024**, *14*, 972. https://doi.org/10.3390/min14100972

Academic Editor: Dave Deglon

Received: 2 September 2024
Revised: 21 September 2024
Accepted: 25 September 2024
Published: 27 September 2024

Copyright: © 2024 by the authors. Licensee MDPI, Basel, Switzerland. This article is an open access article distributed under the terms and conditions of the Creative Commons Attribution (CC BY) license (https://creativecommons.org/licenses/by/4.0/).

1. Introduction

Quartz is a mineral resource with very stable physical and chemical properties, forming the mineral components of various rocks and mineral deposits. It is hard in texture and widely used, often employed in the manufacture of silica gel, water glass, and various silicides and silicates, and it is used as a filler for plastics and rubber. It is also extensively used in the glass, ceramic, petroleum, metallurgy, foundry, and construction material industries. As the demand for quartz minerals continues to increase across various industries, efficiently sorting quartz ore has become very important. Flotation is a commonly used ore sorting method [1–4]. There are two typical methods for quartz flotation [5]. One is direct flotation using cationic amine collectors [6], such as primary amines and their corresponding acetate or chloride derivatives [7]. The other method involves first activating with polyvalent metal ions (such as calcium and magnesium ions) and then using anionic collectors for flotation [8–10], such as sodium oleate, alkyl sulfonates, and alkyl sulfates [11,12]. Currently, due to the wide availability and low cost of long-chain fatty acids and their salts, they are widely used as quartz flotation collectors in the industry. However, these collectors often require heating during the flotation process, raising the slurry temperature above 35 °C, which results in significant energy consumption and is not conducive to environmental protection and energy conservation [13,14].

Therefore, to make the fatty acid collector usable at low temperatures, different functional groups are introduced into the long chain of the fatty acid through chemical reactions to enhance its collecting performance and low-temperature resistance [15]. For example, some scholars have introduced bromine atoms into the α-carbon position to synthesize a new collector, α-bromine fatty acid, using a solvent-free method. At a slurry temperature of 25.0 °C, the collector can obtain an iron concentrate grade of 66.77%, an iron recovery rate of 77.72%, and a tailings iron grade of 8.43% [16,17]. These modified collectors demonstrate satisfactory performance for quartz flotation at low temperatures. However, many synthetic surfactants cause some harm to the environment. For example, the modified fatty acid collectors containing halogen atoms and the commonly used cationic amine collectors will have problems such as difficult degradation and biocompatibility [18,19]. The growing need for eco-friendly products significantly propels the advancement of surfactants. Surfactants with lower toxicity to oceanic ecosystems and that biodegrade faster appear in people's sight, and amino acid surfactants are one of them [20]. Amino acid, a kind of natural group, can create the polar head group in amphiphilic substances, which is multifunctional, non-toxic, and biodegradable. It has broad application prospects in the fields of food, medicine, mineral processing, and wastewater treatment [21,22]. For instance, Sun and colleagues created a novel surfactant made of dicarboxylic amino acids, utilizing glutamic acid and n-capric acid as substrates, and achieved the targeted flotation process to separate manganese ore from quartz and calcite [23]. Karlkvist et al. produced a range of dicarboxylic surfactants, varying in the spacing among carboxylic acid groups (be it one, two, or three methylides), to achieve specific flotation of calcite and apatite [24]. Some scholars used a novel amino acid surfactant, N-lauroylsarcosinate, as an innovative fluorite collector to selectively separate fluorite and scheelite, bypassing the need for depressants [25]. Jia et al. also used the biosurfactant sodium N-lauroylsarcosinate as a new green collector, which improved the flotation efficiency of heteropolar ore from quartz [26].

Based on previous studies, it has been found that the oxygen and nitrogen atoms of the carboxyl group and amine group in amino acids serve as the primary sites for mineral surface adsorption. These active sites can chelate with Cu (II), Ni (II), Co (II), Pd (II), and Sn (II). Some amino acids also have amide groups and can form intermolecular hydrogen bonds with water molecules, which will increase the solubility of these amino acids, which is conducive to the flotation of collectors at low temperatures [27].

Lauroyl lysine (Figure 1) is a novel amino acid-based surfactant synthesized from lauric acid and lysine. It possesses excellent biodegradability, antioxidant properties, and environmental friendliness, and it is commonly used in cosmetics, biomedicine, electroplating, and other fields [28,29]. The presence of three functional groups of amide, primary amine, and carboxyl in structure could give LL greater polarity, higher collecting capacity, and greater low-temperature solubility. However, relevant research on LL in the field of quartz flotation at low temperatures has not been reported. Additionally, the flotation ability and potential adsorption mechanism at low temperatures are still unknown and need to be studied systematically.

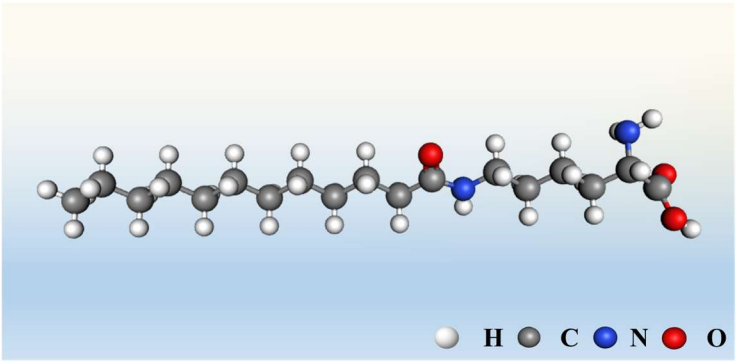

Figure 1. Schematic diagram of the molecular structure of LL.

In this study, LL is a collector in the process of flotation at low temperatures for quartz. The flotation performance of LL at low temperatures is studied by micro-flotation tests and compared to that of NaOL. Furthermore, the low-temperature adsorption process of LL on quartz surfaces is examined using methods like the zeta potential test, adsorption measurements, Fourier transform infrared spectroscopy (FT-IR), scanning electron microscope (SEM) measurements, and X-ray photoelectron spectroscopy (XPS).

2. Experimental

2.1. Materials

The pure quartz samples from the Anshan iron ore in Liaoning, China, were meticulously selected, crushed, and wet-screened for subsequent micro-flotation testing. As shown in Table 1 and Figure 2, the results of the sample's X-ray fluorescence (XRF), X-ray diffraction (XRD), and particle size distribution indicate that the quartz purity is 99.82%, the mineral particle size is approximately −0.14 + 0.014 mm, and the D50 size is approximately 0.070 mm, meeting the requirements for pure mineral flotation.

The collector used in the experiment was an amphoteric collector containing secondary amine and carboxyl groups, namely, N-Lauroyl-Lysine (abbreviated as LL), which was procured from Shanghai McLean Biochemical Technology Co., Ltd. (Shanghai, China), with a purity of 98%. The molecular structure is depicted in Figure 1. The AR-grade sodium oleate and activator analytically pure calcium chloride ($CaCl_2$) were purchased from Sinopharm Chemical Reagent Co., Ltd. (Shanghai China). The pH value of the HCl and NaOH solutions is 0.10 mol/L. In addition, ultra-pure water (18.25 MΩ·cm) was used in all experiments.

Table 1. Chemical composition of the single quartz (wt.%).

SiO_2	Al_2O_3	Na_2O	K_2O	MgO	Fe_2O_3	CaO	Loss
99.82	0.062	0.020	0.021	0.0062	0.014	0.0127	0.0441

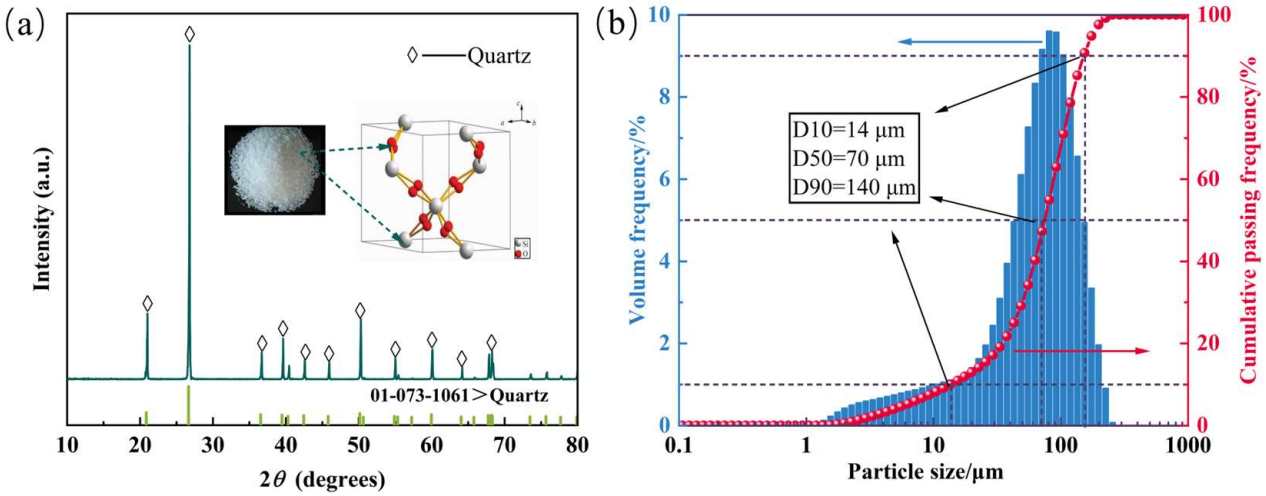

Figure 2. X-ray diffraction spectra of quartz (**a**) and the particle size distribution of quartz (**b**).

2.2. Flotation Tests

Micro-flotation experiments took place within a 40 mL flotation cell of an $XFG_{II}50$ lab flotation device (Jilin Prospecting Machinery Plant, Jilin China). The flotation process is illustrated in Figure 3a. A quartz specimen weighing 2 g was placed in a flotation cell containing deionized water. While agitating the pulp for three minutes at a speed of 1992 rpm, the cell was continuously infused with a pH regulator (H_2SO_4 and NaOH), activator ($CaCl_2$), and collector (NaOL and LL) every 3 min, with an air intake of 0.04 m^3/h, followed by a 4 min flotation process. Each test was repeated three times, and the average

value was reported as the final value. The schematic diagram of the micro-flotation apparatus is shown in Figure 3b, which is similar to that reported in our previous work [30]. Our lab has assembled a miniature flotation cell with a design jacket that allows the water to circulate with the pulp to transfer energy. Using a low-temperature bath as a water bath source to change the temperature of the slurry, the slurry temperature can be adjusted within a certain range of −5~100 °C, and the accuracy is 0.05 °C. The built-in cryo-bath circulation pump provides adequate water circulation to the system, connected to the flotation cell via a rubber hose at a flow rate of 4 L/min. In addition, a separate thermostatic heater is equipped to heat water or reagents if required. Micro-flotation tests can be carried out at stable temperatures (10 °C, 25 °C and 40 °C) with an error within ±0.5 °C.

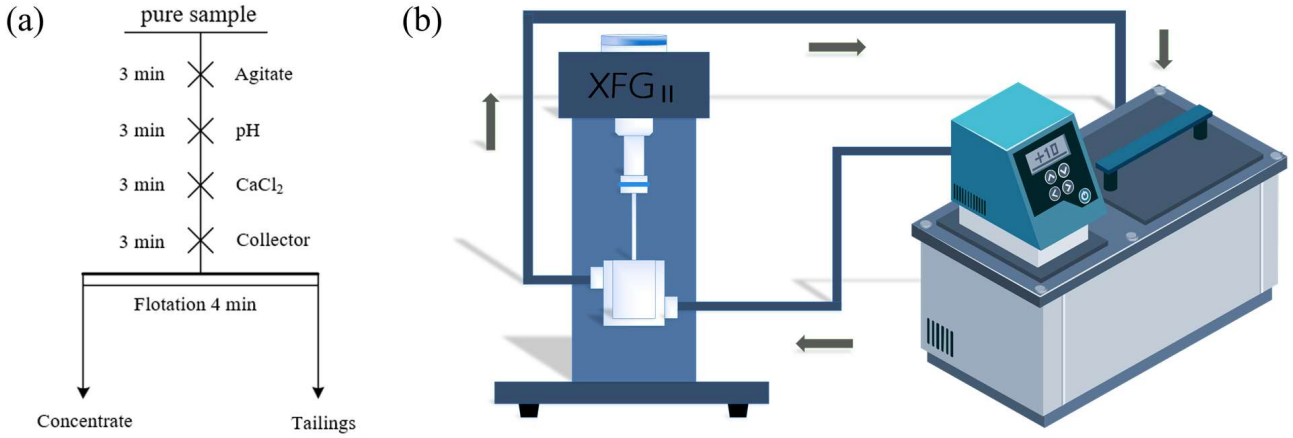

Figure 3. The flotation process of micro-flotation (**a**) and the micro-flotation apparatus schematic diagram (**b**).

2.3. Adsorption Measurement

Total organic carbon (TOC) is widely applied in most flotation studies as a common adsorption measurement method [31,32]. The adsorption measurements were performed using a TOC-LCPH-type total organic carbon analyzer (SHIMADZU Japan, Kyoto Japan). Mineral samples (2 g) were transferred into a 100 mL conical flask containing approximately 40 mL of deionized water. After adding different concentrations of collectors and adjusting the pH, the suspension was stirred magnetically for 15 min and then allowed to stand to let the supernatant be absorbed through a filter with a pore size of 0.45 μm to obtain the sample for measurement [33]. During the process, the temperature was controlled at 10.0 °C. Each group of samples was tested twice. If the error was more than 3%, the third test was conducted, and the average of the two groups with similar results was taken as the result.

First, the standard sample was tested, and the standard curve as shown in Figure 4 was established. As can be seen from Figure 4, the fitting results are satisfactory enough, and the correlation is 0.99833. The resulting fitting equation is $y = 0.32000x - 0.09937$, where x is the LL concentration (mg/L) and y is the TOC concentration of the sample (mg/L).

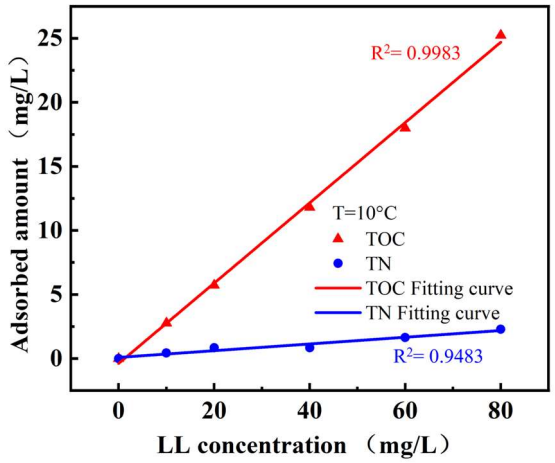

Figure 4. The TOC fitting curve of standard samples.

2.4. SEM-EDS Measurement

A scanning electron microscope (Phenom Prox, Thermo Scientific, Bleiswijk, The Netherlands), fitted with an energy dispersive X-ray spectrometer (EDS), was utilized to examine the surface structure and makeup of quartz treated with a collector. The functional voltage ranged between 5 and 15 kV [34,35]. Two grams of pure quartz was introduced into 50 mL of deionized water containing $CaCl_2$ and LL, under a pH of 11 and a temperature of 10 °C. Following a 0.5 h stirring period, the pulp underwent filtration and drying.

2.5. Zeta Potential Measurements

Zeta potentials were measured by a Zetasizer Nano ZS90 analyzer (Malvern Panalytical, Malvern Britain) at 10 °C. The quartz sample (20.0 mg) to be measured was ground to −0.005 mm and placed into a 1×10^{-3} mol/L KCl background electrolyte solution. The zeta potential on the surface of the sample was measured with or without $CaCl_2$ and collector LL. The pH of the pulp was adjusted with the configured HCl/NaOH solution. The upper clarified liquid was added to the electrophoresis tank after standing. Each sample was measured 3 times (with an experimental error of less than 2.0%), and the average value was taken for analysis.

2.6. Fourier Transform Infrared Spectroscopy

In the FT-IR detection of collector LL, a glass rod was used to submerge the samples into the KBr slice to analyze the infrared spectrum through FT-IR spectroscopy (Frontier, PerkinElmer, Shelton USA). The samples used for FT-IR analysis were prepared as follows: A mixture of 2 g of quartz, 20 mg/L $CaCl_2$, and 60 mg/L LL was introduced into 50 mL of deionized water, maintained at a pH of 11 and a temperature of 10 °C. Following a 0.5 h stirring period, the pulp underwent filtration, rinsing, and subsequent drying in a vacuum oven.

2.7. X-ray Photoelectron Spectroscopy

XPS technology was employed to identify the elemental makeup, chemical condition, and photoelectron binding energy of various atoms present on mineral surfaces [36,37]. The mineral samples were processed by the same procedure as in the FT-IR measurement. An analysis of the collected samples was conducted with a versatile scanning imaging photoelectron spectrometer (PHI5000 Versa Probe II, ULVAC-PHI, Inc., Kanagawa Japan), characterized by its 50 W power, 15 kV voltage, Al target anode, and carbon atom calibration for the atom binding energy (C 1s: 284.8 eV).

3. Results and Discussion

3.1. Micro-Flotation Tests

The influence of the pH of the pulp on the recovery of quartz flotation at 25 °C, with collector LL and NaOL at 60.0 mg/L and $CaCl_2$ at 20.0 mg/L, is illustrated in Figure 5a. When LL is a collector for the flotation of quartz, at the pulp pH of 11.04, the quartz flotation recovery reaches 98.47%, and NaOL as a collector reveals an upward trend in recovery correlating with the rise in pulp pH. As the pH is less than 7.0, the flotation recovery of quartz by NaOL is very low. With the pulp pH exceeding 7.0, the recovery of quartz rose, which gradually increased to more than 80.00%. In summary, it was shown that LL has a strong ability to collect quartz under alkaline conditions, which is greater than that of NaOL.

The impact of the LL and NaOL concentration on quartz recovery was analyzed, with the findings presented in Figure 5b. When employing LL as the collector, the recovery markedly rises from 54.75% to 98.90%, with a pulp pH of 11.0, a $CaCl_2$ concentration of 20.0 mg/L, and a varying LL concentration between 15–80 mg/L. Furthermore, when the concentration of LL is greater than 45 mg/L, the recovery has no obvious change. In contrast, when the NaOL is 60 mg/L, the recovery is the highest, reaching 82.41%. When the amount of NaOL exceeded 60 mg/L, the recovery of quartz began to decline, which is speculated to be due to the high concentration of NaOL that produced multi-layer adsorption, resulting in the decrease in quartz surface hydrophobicity [38]. In summary, the collecting capacity of LL is stronger than NaOL.

As shown in Figure 5c, the effect of activator $CaCl_2$ on the recovery was studied. With the pulp pH at 11.0 and LL concentration at 60 mg/L, the recovery rate rose from 4.17% to 97.25% as the $CaCl_2$ concentration went up from 0 to 20 mg/L. Then, the recovery had no significant change with the concentration of $CaCl_2$ further increasing to 60.0 mg/L. A similar trend is observed when NaOL is used as the collector. To ensure the activation effect of $CaCl_2$, 20 mg/L $CaCl_2$ is selected as the activator concentration.

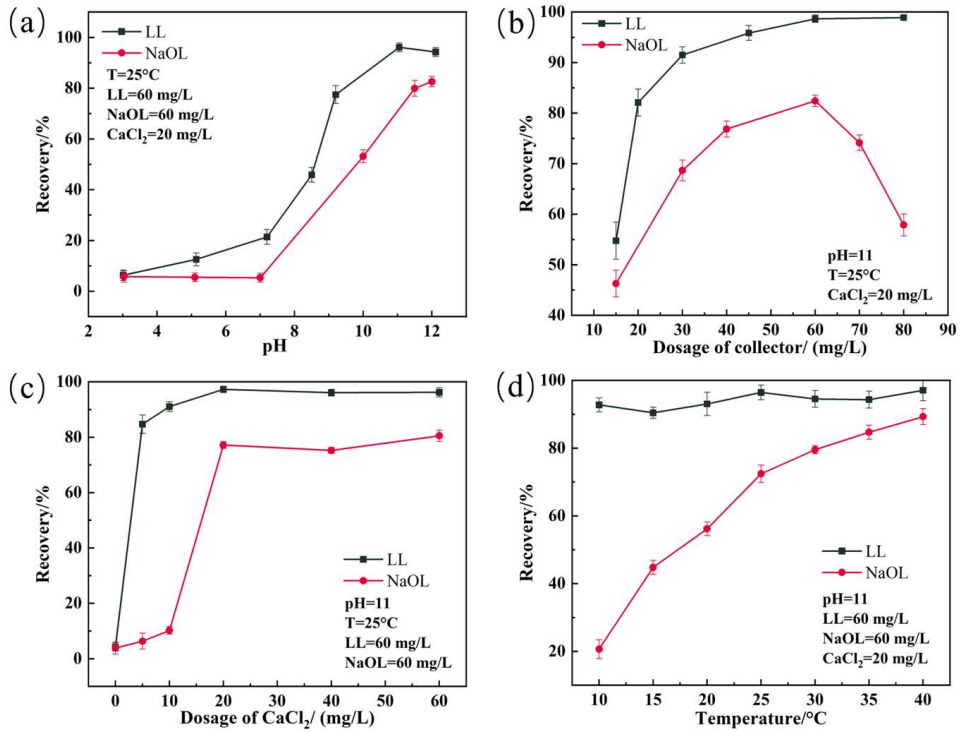

Figure 5. Recoveries of quartz as a function of pH (**a**), collector concentration (**b**), $CaCl_2$ concentration (**c**), and pulp temperature (**d**).

As shown in Figure 5d, the influence of the pulp temperature on the recovery is studied when sodium oleate and LL are used as collectors, respectively. When the pulp pH stands at 11.0, with LL and NaOL at 60 mg/L and $CaCl_2$ at 20 mg/L, the temperature at which flotation occurs little impacts the LL collection efficiency. Across the pulp temperature (10–40 °C), the recovery stays over 91%. The pulp temperature has a significant effect on the collection capacity of NaOL. The flotation of quartz by NaOL is difficult when the temperature falls below 20 °C. The recovery is 89.29% by NaOL at 40 °C.

The results of micro-flotation experiments show that the new collector LL has a strong collecting ability in a wide temperature range.

3.2. TOC Measurement Results

Figure 6 shows that the TOC and total nitrogen (TN) in the collector adsorbed on the quartz surface increased with the expansion of the collector concentration, reaching a peak value when the collector dosage was 60 mg/L, which is consistent with the micro-flotation results. The results of the adsorption measurement prove that the collector is adsorbed on the quartz surface at T = 10 °C, indicating that LL has the potential to exhibit better collection performance in quartz flotation at low temperatures.

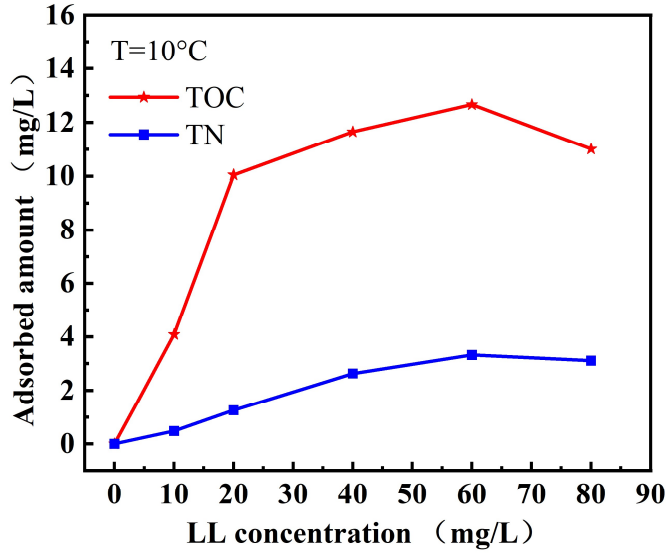

Figure 6. The adsorption results of quartz with the TOC method.

3.3. SEM-EDS Measurements

A series of SEM-EDS probe analyses are conducted to observe the surface structure of untreated versus treated quartz with LL and $CaCl_2$, aiming to comprehend the nature and spread of LL on the quartz surface [39]. SEM images and microchemical mappings of the chosen quartz region (Figure 7) exhibitions are made before and following treatment with LL and $CaCl_2$. As depicted in Figure 7a,b, the quartz surface, untreated with LL and $CaCl_2$, appears notably even and level, with the microchemical mapping of the chosen region revealing a dense and symmetrical distribution of oxygen and silicon elements on the surface. However, noticeable granular materials are present on the quartz surface after LL treatment (Figure 7c,d). The microchemical map of the selected region clearly shows the presence of carbon, calcium, and nitrogen. These results demonstrate that LL is tightly absorbed on the quartz surface [6,36].

The results of EDS mapping in the adsorbed quartz sample confirm the presence of 8.283% nitrogen, 30.757% carbon, and 0.122% calcium, which also confirms the adsorption of LL after being adjusted with $CaCl_2$ on the quartz (Table 2) [40].

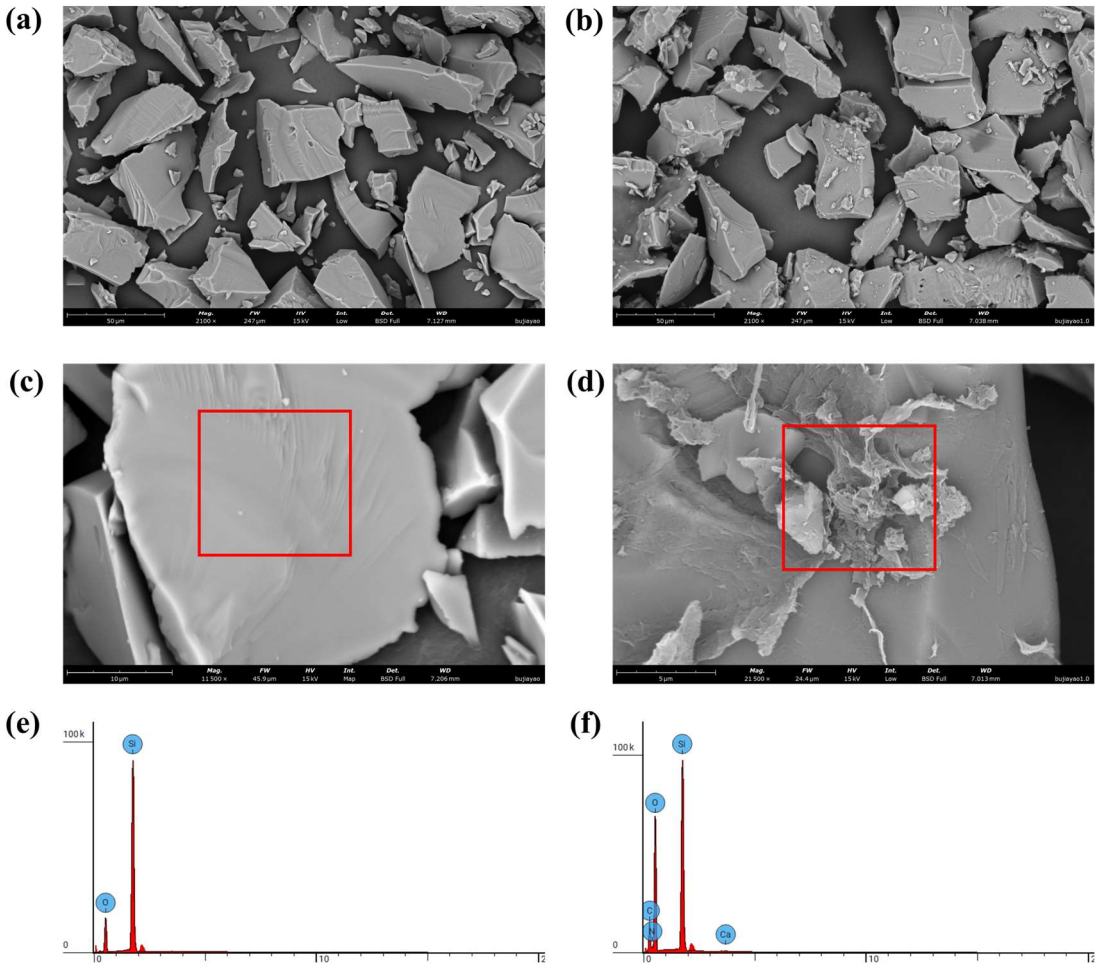

Figure 7. (**a**) Surface morphology of quartz, (**b**) surface morphology of quartz treated with LL and $CaCl_2$, (**c**,**d**) local magnification, and (**e**,**f**) EDS mapping.

Table 2. The surface atomic compositions (at.%) of quartz by EDS.

Element	Atomic Conc.%				
	Si	O	C	N	Ca
Quartz	57.064	42.936	-	-	-
Quartz + $CaCl_2$ + LL	14.256	46.582	30.757	8.283	0.122

3.4. Zeta Potential Analyses

Changes in the zeta potential of mineral surfaces may indicate how collectors affect these minerals, and thus it is often used to help elucidate how active sites on mineral surfaces are adsorbed [41–43]. Figure 8a shows the variation trend of the zeta potential on quartz surfaces under varying pH levels. In the range of pH 2 to 14, the zeta potential is negative. As pH levels increase, the zeta potential consistently decreases. The increase in pH levels leads to a greater absorption of OH^- ions on the quartz surface's dual layer [44].

Following treatment with 20 mg/L $CaCl_2$ (Figure 8b), due to the calcium ions in the pulp being Ca^{2+} and $Ca(OH)^+$ during flotation, absorbed on the quartz's negative surface, the zeta potential on the quartz surface rises following activation by $CaCl_2$ [8].

Figure 8c illustrates the alterations in zeta potential on quartz surfaces after being treated with $CaCl_2$ and LL. As the pH level is about 4~12, there is a reduction in the zeta potential of the chemical-treated quartz surface [6,45]. Because the collector ($RCOO^-$) reacts with the $Ca(OH)^+$ in the solution, and the product RCOO—Ca(OH) reacts with the

-Si-OH group on the quartz surface through chemisorption; therefore, its zeta potential decreases, which is consistent with the flotation results [46].

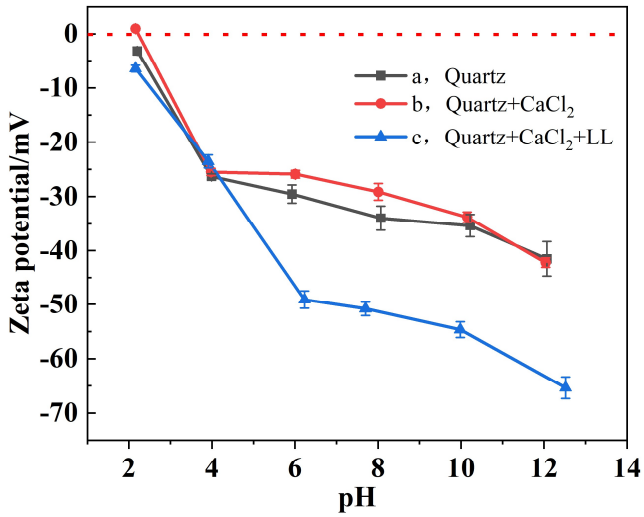

Figure 8. The zeta potentials of quartz with respect to pH (T = 10 °C, $CaCl_2$ 20 mg/L, LL 60 mg/L).

3.5. Fourier Transform Infrared Analyses

FT-IR spectroscopy is utilized to examine the adsorption of collector LL onto the quartz surface. As depicted in Figure 9a of the FT-IR spectra for quartz, the peak at 1085 cm^{-1} is ascribed to the Si-O-Si asymmetric stretching vibration, marking quartz's first characteristic absorption peak [16]. The observed peaks around 782, 471, and 688 cm^{-1} are indicative of the symmetrical stretching of Si-O-Si [45].

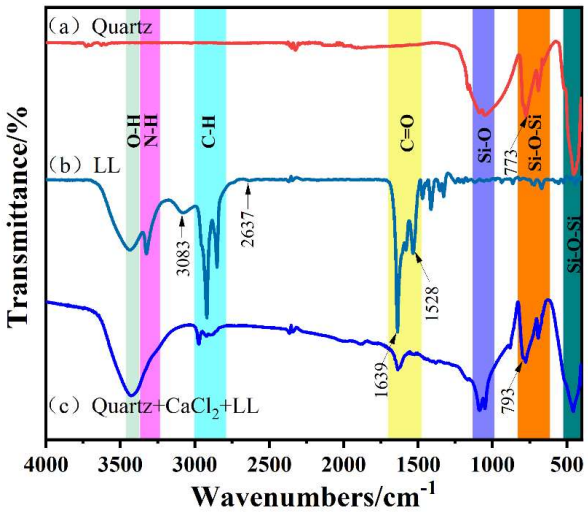

Figure 9. The FT-IR spectral analysis of quartz samples (a), LL (b), and quartz treated with LL and $CaCl_2$ (c).

As depicted in Figure 9b of the FT-IR spectra for LL, the peak at 3322 cm^{-1} is sharp, which is the stretching vibration peak of N-H on secondary amide; 2980 and 2900 cm^{-1} corresponded to asymmetric and symmetric contraction vibrations of $-CH_3$ and $-CH_2$ groups, respectively. The peaks near 1528 cm^{-1} belong to the C-N stretching vibration of secondary amide mixed with the bending vibration of N-H, belonging to the amide II band. The peak near the positions of 3083 cm^{-1} and 2637 cm^{-1} is attributed to the $-NH_3^+$ vibration absorption peak. Due to the influence of hydrogen bonding, the location of the C=O stretching vibration absorption peak in carboxylic acid shifts to the lower wave number, emerging around 1649 cm^{-1} [28,47].

Figure 9c displays the infrared spectrum for quartz dealt with $CaCl_2$ and LL, where 2981 cm^{-1} and 2900 cm^{-1} correspond to the asymmetric stretching vibrations of the -CH_3 and -CH_2 groups, respectively, indicating that LL adsorbs on the activated quartz surface [48]. Additionally, the locations of those peaks are noticeably altered when contrasted with the LL and initial quartz. The peaks of -CH_3 and -CH_2 exhibit shifts of approximately about 62 cm^{-1} and 40 cm^{-1}. Si-O-Si symmetrical stretching vibration moves from 793 cm^{-1} to 771 cm^{-1}. Such occurrences reveal that there is a chemical adsorption happening between LL and the surface of quartz. Additionally, the observed peak at 3430 cm^{-1} is attributed to the -NH/-OH stretching vibration absorption peaks, signifying hydrogen bonding adsorption [16,17,49].

3.6. XPS Analyses

Figure 10a and Table 3 display the XPS spectrum outcomes for quartz and quartz dealing with LL and $CaCl_2$. The peak of C (1s) at 284.8 eV in quartz XPS spectra is ascribed to environmental hydrocarbon pollution [50]. Furthermore, the observed peaks near 103 eV and 532 eV correspond to the existence of silicon and oxygen [51]. After dealing with LL and $CaCl_2$, it is observed that N (1s, 3.66 at.%, 399.30 eV) is absorbed into the quartz surfaces [45]. Additionally, the levels of Si (2p) and O (1s) fell by 10.52 at.% and 15.05 at.%, and the concentration of C (1s) rose by 23.03 at.% relative to the original quartz surface.

For a deeper exploration of LL adsorption on quartz, Figure 10 illustrates the curve fitting of C (1s), O (1s), and Si (2p) peaks [52]. Figure 10b reveals the presence of two novel components at 286.23 eV, attributable to the C-O-C bonds, and 288.49 eV, attributable to the carboxylate group [17,50,53]. In addition, the C-C bond peak intensity at 284.8 eV increases significantly. This suggests that collector LL has successfully absorbed onto the surface of quartz.

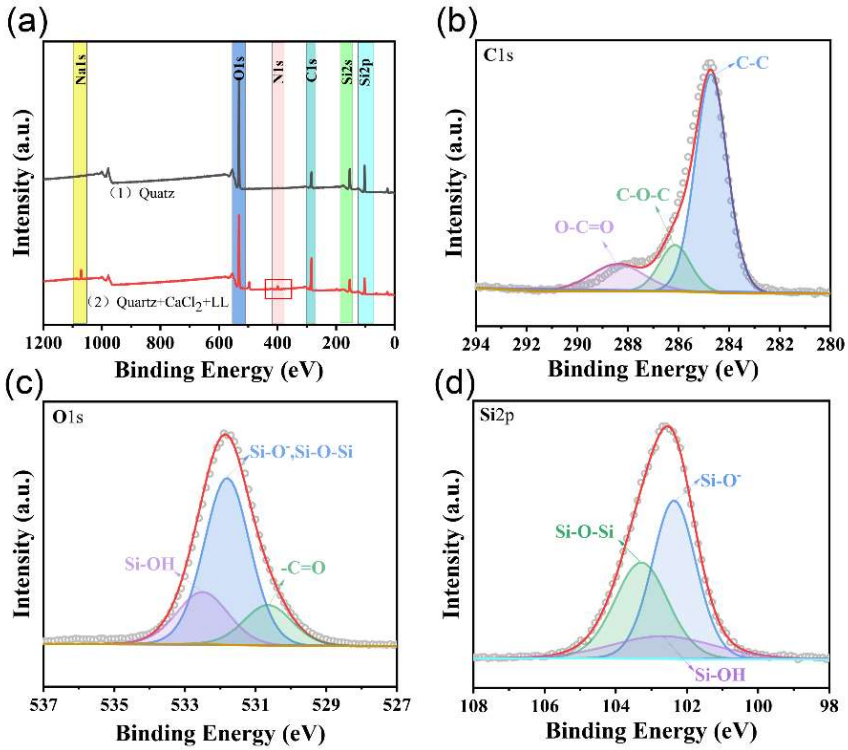

Figure 10. (**a**) The XPS full spectrum, (**b**) the high resolution of C 1s, (**c**) the high resolution of O 1s, (**d**) the high resolution of Si 2p.

As shown in Figure 10c, peaks at 530.65 eV, 531.81 eV, and 532.50 eV are identified in the O1s signals, corresponding to Si-O^-/Si-O-Si and Si-OH, in that order [16,53,54]. Following treatment with $CaCl_2$ and LL, a novel component at 530.65 eV, attributed to the

-C=O bond, is identified [45]. Furthermore, due to the fact that LL molecules adsorb on the mineral surface, the Si-OH oxygen line intensity on the quartz surface falls from 49.31% to 39.09%. Such occurrences suggest that the LL is capable of adsorbing into the activated quartz surface.

As shown in Figure 10d, the Si(2p) peak is deconvoluted at 102.36, 102.67, and 103.28 eV (Table 3), which are assigned to Si atoms in Si-O^-, Si-OH, and Si-O-Si bonds. Moreover, the intensity of the silicon line on the quartz surface decreases from 32.44% to 18.77%, suggesting that the collector absorbs the quartz surface through hydrogen bond force. These phenomena reflect that the LL could adsorb onto the activated quartz surface [54–57].

Table 3. Relative contents of elements on the surface of quartz by XPS.

Sample	Element at.% (BE, eV)			
	C	O	Si	N
Quartz	16.84 (284.8)	41.32 (531.71)	22.72 (102.32)	-
	-	7.99 (532.46)	9.72 (103.35)	-
Quartz + $CaCl_2$ + LL	28.13 (284.8)	6.23 (530.65)	9.09 (102.36)	3.66 (399.30)
	5.73 (286.23)	24.36 (531.81)	2.99 (102.67)	-
	5.83 (288.49)	8.50 (532.50)	6.69 (103.28)	-

Integrated with the analytical findings from SEM/EDS, FT-IR, XPS, and the zeta potential, the adsorption process of LL on quartz at low temperatures is inferred, as shown in Figure 11. Initially, calcium ions are adsorbed by electrostatic forces to the negatively charged quartz surface, resulting in the activation of the quartz surface by calcium ions. Then, owing to the intense chemical interplay between Ca and O, the collector adsorbs to the quartz surface. Additionally, the formation of a hydrogen bond between the collector's primary amine molecules and the quartz surface enhances the collector adsorption stability at low temperatures [46]. The amide groups in the LL molecular structure may increase the solubility of the collector at low temperatures, and the amide bonds are capable of creating hydrogen bonds between oxygen and hydrogen molecules, enhancing their hydrophobicity [23]. Therefore, LL manifests a strong ability to collect quartz at low temperatures.

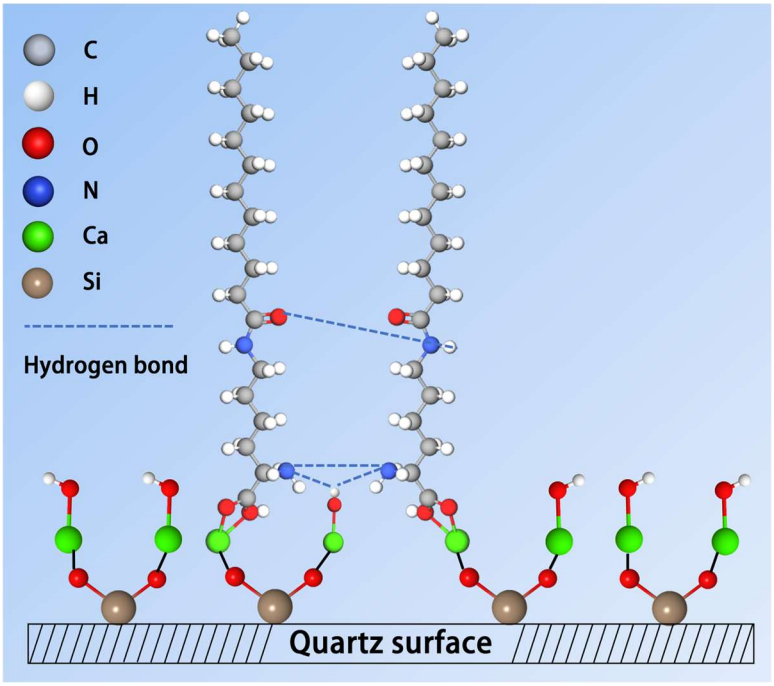

Figure 11. The adsorption models of LL on quartz surface at low temperature.

4. Conclusions

In this study, the new amino acid surfactant LL is used as a collector for quartz flotation at low temperatures. The experimental results show that LL is an efficient collector and has excellent collection performance in quartz flotation even at low temperatures. According to the results of micro-flotation experiments, the temperature of the pulp little impacts LL collection efficiency, and the highest recovery of quartz flotation is 97.08% at pH = 11.0, $CaCl_2$ = 20 mg/L, and LL = 60 mg/L. On the contrary, NaOL exhibits subpar results in quartz flotation when the temperature is under 20 °C. Findings from TOC and SEM studies reveal the effective adsorption of collector LL onto the quartz surface under cold conditions. Findings from zeta potentials, X-ray photoelectron spectroscopy (XPS) analysis, and Fourier transform infrared (FT-IR) spectra studies reveal that LL is adsorbed to the surface of activated quartz through chemical adsorption. Furthermore, the creation of a hydrogen bond between the primary amine and the quartz surface enhances the collector collecting capacity. The amide groups in the LL structure may increase their solubility to improve mineral flotation at low temperatures. The amide bonds in the LL structure can create hydrogen bonds between oxygen and hydrogen molecules to enhance their hydrophobicity and then improve the flotation recovery of quartz.

Author Contributions: F.W.: Investigation, Methodology, Writing—original draft. S.C.: Investigation, Validation, Writing—review and editing, Funding acquisition. W.Y.: Conceptualization, Methodology. Y.F.: Methodology, Visualization. C.L.: Conceptualization, Methodology. Y.C.: Supervision. All authors have read and agreed to the published version of the manuscript.

Funding: The authors are thankful for the support of the Hebei Provincial Central Guidance Local Science and Technology Development Project (Grant No. 236Z4109G).

Data Availability Statement: The data presented in this study are available on request from the corresponding author.

Conflicts of Interest: Yafeng Fu is an employee of Ansteel Beijing Research Institute Co., Ltd. The paper reflects the views of the scientists and not the company.

References

1. Li, W.; Zhou, L.; Han, Y.; Zhu, Y.; Li, Y. Effect of carboxymethyl starch on fine-grained hematite recovery by high-intensity magnetic separation: Experimental investigation and theoretical analysis. *Powder Technol.* **2019**, *343*, 270–278. [CrossRef]
2. Yang, L.; Li, X.; Li, W.; Yan, X.; Zhang, H. Intensification of interfacial adsorption of dodecylamine onto quartz by ultrasonic method. *Sep. Purif. Technol.* **2019**, *227*, 115701. [CrossRef]
3. Jia, K.; Ding, R.; Chen, Y.; Lu, T.; Li, G.; Cao, Y.; Wang, C. Green, multiple-ligand collector sodium myristoyl glutamate for flotation of smithsonite. *Appl. Surf. Sci.* **2024**, *660*, 159932. [CrossRef]
4. Yang, B.; He, J. New insights into selective depression mechanism of Tamarindus indica kernel gum in flotation separation of fluorapatite and calcite. *Sep. Purif. Technol.* **2025**, *354*, 128787. [CrossRef]
5. Deng, J.; Yang, S.; Liu, C.; Li, H. Effects of the calcite on quartz flotation using the reagent scheme of starch/dodecylamine. *Colloids Surf. Physicochem. Eng. Asp.* **2019**, *583*, 123983. [CrossRef]
6. Liu, W.; Liu, W.; Dai, S.; Wang, B. Adsorption of bis(2-hydroxy-3-chloropropyl) dodecylamine on quartz surface and its implication on flotation. *Results Phys.* **2018**, *9*, 1096–1101. [CrossRef]
7. Cheng, Z.; Zhu, Y.; Li, Y.; Han, Y. Flotation and adsorption of quartz with the new collector butane-3-heptyloxy-1,2-diamine. *Mineral. Petrol.* **2019**, *113*, 207–216. [CrossRef]
8. Gong, G.; Liu, J.; Han, Y.; Zhu, Y. An atomic scale investigation of the adsorption of sodium oleate on Ca^{2+} activated quartz surface. *Physicochem. Probl. Miner. Process.* **2019**, *55*, 426–436.
9. Wang, L.; Wang, G.; Ge, P.; Sun, W.; Tang, H.; Hu, W. Activation mechanisms of quartz flotation with calcium ions and cationic/anionic mixed collectors under alkalescent conditions. *Colloids Surf. Physicochem. Eng. Asp.* **2022**, *632*, 127771. [CrossRef]
10. Sun, H.; Wang, Y.; Wang, D.; Yin, W.; Yao, J. Selective adsorption analysis of BAPTA depressants on the surface of carbonate minerals: Insights into flotation behavior and adsorption mechanism. *Surf. Interfaces* **2024**, *45*, 103872. [CrossRef]
11. Wang, M.; Jin, S. Utilization of Phytic Acid as a Selective Depressant for Quartz Activated by Zinc Ions in Smithsonite Flotation. *Molecules* **2023**, *28*, 5361. [CrossRef] [PubMed]
12. Zheng, Q.; Zhou, Y.; Qiao, L.; Shen, P.; Mao, Y.; Dong, L.; Liu, D. Selective adsorption of soluble starch on the cassiterite surface for effective flotation separation of scheelite from cassiterite. *Surf. Interfaces* **2024**, *48*, 104238. [CrossRef]
13. Ren, L.; Qiu, H.; Zhang, Y.; Nguyen, A.V.; Zhang, M.; Wei, P.; Long, Q. Effects of alkyl ether amine and calcium ions on fine quartz flotation and its guidance for upgrading vanadium from stone coal. *Powder Technol.* **2018**, *338*, 180–189. [CrossRef]

14. Nakhaei, F.; Irannajad, M. Reagents types in flotation of iron oxide minerals: A review. *Miner. Process. Extr. Metall. Rev.* **2018**, *39*, 89–124. [CrossRef]
15. Ogata, Y.; Sugimoto, T.; Inaishi, M. α-Chlorination of Long-chain Aliphatic Acids. *Bull. Chem. Soc. Jpn.* **1979**, *52*, 255–256. [CrossRef]
16. Luo, B.; Zhu, Y.; Sun, C.; Li, Y.; Han, Y. Flotation and adsorption of a new collector α-Bromodecanoic acid on quartz surface. *Miner. Eng.* **2015**, *77*, 86–92. [CrossRef]
17. Zhu, Y.; Luo, B.; Sun, C.; Li, Y.; Han, Y. Influence of bromine modification on collecting property of lauric acid. *Miner. Eng.* **2015**, *79*, 24–30. [CrossRef]
18. Asgari, K.; Huang, Q.; Khoshdast, H.; Hassanzadeh, A. A Review on Bioflotation of Coal and Minerals: Classification, Mechanisms, Challenges, and Future Perspectives. *Miner. Process. Extr. Metall. Rev.* **2024**, *45*, 46–76. [CrossRef]
19. Mishra, S.; Panda, S.; Akcil, A.; Dembele, S. Biotechnological Avenues in Mineral Processing: Fundamentals, Applications and Advances in Bioleaching and Bio-beneficiation. Miner. *Process. Extr. Metall. Rev.* **2023**, *44*, 22–51. [CrossRef]
20. Bordes, R.; Holmberg, K. Amino acid-based surfactants—Do they deserve more attention? *Adv. Colloid Interface Sci.* **2015**, *222*, 79–91. [CrossRef]
21. Zhang, C.; Wu, D.; Qiu, X. Stimulatory effects of amino acids on γ-polyglutamic acid production by Bacillus subtilis. *Sci. Rep.* **2018**, *8*, 17934. [CrossRef] [PubMed]
22. Khoso, S.A.; Hu, Y.; Lyu, F.; Liu, R.; Sun, W. Selective separation of chalcopyrite from pyrite with a novel non-hazardous biodegradable depressant. *J. Clean. Prod.* **2019**, *232*, 888–897. [CrossRef]
23. Sun, H.; Wang, S.; Fei, L.; Cao, Z.; Zhong, H.; Ma, X. The selective flotation separation of rhodochrosite against quartz and calcite with dicarboxylic amino acid-based surfactants as a novel collector. *Miner. Eng.* **2022**, *182*, 107559. [CrossRef]
24. Karlkvist, T.; Patra, A.; Rao, K.H.; Bordes, R.; Holmberg, K. Flotation selectivity of novel alkyl dicarboxylate reagents for apatite–calcite separation. *J. Colloid Interface Sci.* **2015**, *445*, 40–47. [CrossRef]
25. Gao, Z.; Jiang, Z.; Sun, W.; Pooley, S.G.; Wang, J.; Liu, Y.; Xu, F.; Wang, Q.; Zeng, L.; Wu, Y. New role of the conventional foamer sodium N-lauroylsarcosinate as a selective collector for the separation of calcium minerals. *J. Mol. Liq.* **2020**, *318*, 114031. [CrossRef]
26. Jia, K.; Lu, Y.; Liu, J.; Cheng, S.; Liu, S.; Cao, Y.; Li, G. Selective flotation separation of hemimorphite from quartz using the biosurfactant sodium N-lauroylsarcosinate as a novel collector. *Miner. Eng.* **2023**, *198*, 108073. [CrossRef]
27. Liu, J.; Liu, W.; Wang, Y.; Xu, M.; Wang, B. A novel reusable nanocomposite adsorbent, xanthated Fe3O4-chitosan grafted onto graphene oxide, for removing Cu(II) from aqueous solutions. *Appl. Surf. Sci.* **2016**, *367*, 327–334. [CrossRef]
28. Wang, Y.; Liu, Y.; He, Y.; Huang, J.; Xu, H. Preparation of Pickering emulsion stabilized by lauroyl lysine. *Tenside Surfactants Deterg.* **2023**, *60*, 21–35. [CrossRef]
29. Gesslein, B.W.; Oshimura, E.; Popova, K. Water Dispersible Lauroyl Lysine in Cleansing Applications. SOFW J. *Int. J. Angew. Wiss.* **2014**, *140*, 32, 34–36.
30. Cao, S.; Yin, W.; Yang, B.; Zhu, Z.; Sun, H.; Sheng, Q.; Chen, K. Insights into the influence of temperature on the adsorption behavior of sodium oleate and its response to flotation of quartz. *Int. J. Min. Sci. Technol.* **2022**, *32*, 399–409. [CrossRef]
31. Wang, Y.; Li, Y.; Xia, W.; Peng, Y.; Xie, G. Adsorption of sodium oleate on coal surface with different oxidation degrees and its effect on flotation. *Colloids Surf. Physicochem. Eng. Asp.* **2021**, *611*, 125801. [CrossRef]
32. Kuang, J.; Zou, Z.; Huang, Z.; Liu, P.; Yuan, W.; Zhu, L. Surface dissolution of scheelite under different regulators and its effect on flotation behavior. *Miner. Eng.* **2021**, *164*, 106811. [CrossRef]
33. Gao, Y.; Fu, X.; Yue, T.; Sun, W. A novel GCMS method for the quantitative analysis of sodium oleate in froth flotation. *Miner. Eng.* **2022**, *176*, 107317. [CrossRef]
34. Schaefer, C.E.G.R.; Gilkes, R.J.; Fernandes, R.B.A. EDS/SEM study on microaggregates of Brazilian Latosols, in relation to P adsorption and clay fraction attributes. *Geoderma* **2004**, *123*, 69–81. [CrossRef]
35. Chelgani, S.C.; Hart, B.; Marois, J.; Ourriban, M. Study of pyrochlore matrix composition effects on froth flotation by SEM–EDX. *Miner. Eng.* **2012**, *30*, 62–66. [CrossRef]
36. Xu, L.; Liu, D.; Sun, R.; Wang, Y.; Liu, Z.; Shao, P.; Wang, C.; Wen, S. Flotation separation of smithsonite and calcite in sodium oleate system using soluble starch as depressant. *Miner. Eng.* **2024**, *205*, 108490. [CrossRef]
37. Yang, B.; Zhu, L.; He, J.; Yin, W.; Yao, J. A feasible strategy for depressant-free flotation separation of siderite from magnesiohornblende using a highly selective collector. *J. Mol. Liq.* **2024**, *394*, 123689. [CrossRef]
38. Zhang, D.; Kang, J.; Zhu, W. Selective flotation separation of fluorite and calcite by utilising a novel anionic/nonionic collector. *Colloids Surf. Physicochem. Eng. Asp.* **2022**, *642*, 128687. [CrossRef]
39. Zhu, Z.; Zhao, B.; Tian, C.; Sheng, Q.; Li, Z.; Zhang, N.; Wang, J.; Yang, X. Polyaspartic acid, an eco-friendly regulator for the improvement of coking coal flotation: Applications and mechanism. *Int. J. Coal Prep. Util.* **2024**, 1–20. [CrossRef]
40. Cherif, O.M.; Bouhenguel, M.; Amirech, A.; Gherraf, N.; Bouchemma, A. Adsorption of tetradecylamine on quartz and its implication on flotation. *Chem. Pap.* **2023**, *77*, 5183–5197. [CrossRef]
41. Yin, Z.; Hu, Y.; Sun, W.; Zhang, C.; He, J.; Xu, Z.; Zou, J.; Guan, C.; Zhang, C.; Guan, Q.; et al. Adsorption Mechanism of 4-Amino-5-mercapto-1,2,4-triazole as Flotation Reagent on Chalcopyrite. *Langmuir* **2018**, *34*, 4071–4083. [CrossRef] [PubMed]
42. Yin, W.; Xue, J.; Li, D.; Sun, Q.; Yao, J.; Huang, S. Flotation of heavily oxidized pyrite in the presence of fine digenite particles. *Miner. Eng.* **2018**, *115*, 142–149. [CrossRef]

43. Liu, C.; Zhou, M.; Xia, L.; Fu, W.; Zhou, W.; Yang, S. The utilization of citric acid as a depressant for the flotation separation of barite from fluorite. *Miner. Eng.* **2020**, *156*, 106491. [CrossRef]
44. Forbes, E.; Bradshaw, D.J.; Franks, G.V. Temperature sensitive polymers as efficient and selective flotation collectors. *Miner. Eng.* **2011**, *24*, 772–777. [CrossRef]
45. Luo, B.; Zhu, Y.; Sun, C.; Li, Y.; Han, Y. The flotation behavior and adsorption mechanisms of 2-((2-(decyloxy)ethyl)amino)lauric acid on quartz surface. *Miner. Eng.* **2018**, *117*, 121–126. [CrossRef]
46. Guo, W.; Han, Y.; Zhu, Y.; Li, Y.; Tang, Z. Effect of amide group on the flotation performance of lauric acid. *Appl. Surf. Sci.* **2020**, *505*, 144627. [CrossRef]
47. Kitadai, N.; Yokoyama, T.; Nakashima, S. In situ ATR-IR investigation of L-lysine adsorption on montmorillonite. *J. Colloid Interface Sci.* **2009**, *338*, 395–401. [CrossRef]
48. Sahoo, H.; Sinha, N.; Rath, S.S.; Das, B. Ionic liquids as novel quartz collectors: Insights from experiments and theory. *Chem. Eng. J.* **2015**, *273*, 46–54. [CrossRef]
49. Guo, W.; Zhu, Y.; Han, Y.; Li, Y.; Yuan, S. Flotation performance and adsorption mechanism of a new collector 2-(carbamoylamino) lauric acid on quartz surface. *Miner. Eng.* **2020**, *153*, 106343. [CrossRef]
50. Liu, W.; Liu, W.; Wei, D.; Li, M.; Zhao, Q.; Xu, S. Synthesis of N,N-Bis(2-hydroxypropyl)laurylamine and its flotation on quartz. *Chem. Eng. J.* **2017**, *309*, 63–69. [CrossRef]
51. Nan, H.; Huang, R.; Zhang, X.; Wang, C. How does ball-milling elevate biochar as a value-added peroxydisulfate activator for antibiotics removal? *Ind. Crops Prod.* **2024**, *214*, 118569. [CrossRef]
52. Zhang, X.; Huang, R.; Show, P.L.; Mahlknecht, J.; Wang, C. Degradation of tetracycline by nitrogen-doped biochar as a peroxydisulfate activator: Nitrogen doping pattern and non-radical mechanism. *Sustain. Horiz.* **2024**, *10*, 100091. [CrossRef]
53. Buckley, A.N.; Parker, G.K. Adsorption of n-octanohydroxamate collector on iron oxides. *Int. J. Miner. Process.* **2013**, *121*, 70–89. [CrossRef]
54. Filippov, L.O.; Severov, V.V.; Filippova, I.V. Mechanism of starch adsorption on Fe–Mg–Al-bearing amphiboles. *Int. J. Miner. Process.* **2013**, *123*, 120–128. [CrossRef]
55. Ray, S.K.; Maiti, C.K.; Lahiri, S.K.; Chakrabarti, N.B. Properties of silicon dioxide films deposited at low temperatures by microwave plasma enhanced decomposition of tetraethylorthosilicate. *J. Vac. Sci. Technol. B Microelectron. Nanometer Struct. Process. Meas. Phenom.* **1992**, *10*, 1139–1150. [CrossRef]
56. Gardner, S.D.; Singamsetty, C.S.K.; Booth, G.L.; He, G.-R.; Pittman, C.U. Surface characterization of carbon fibers using angle-resolved XPS and ISS. *Carbon* **1995**, *33*, 587–595. [CrossRef]
57. Fujita, K.; Oya, A.; Benoit, R.; Beguin, F. Structure and mechanical properties of methyltrimethoxysilane-treated taeniolite films. *J. Mater. Sci.* **1996**, *31*, 4609–4615. [CrossRef]

Disclaimer/Publisher's Note: The statements, opinions and data contained in all publications are solely those of the individual author(s) and contributor(s) and not of MDPI and/or the editor(s). MDPI and/or the editor(s) disclaim responsibility for any injury to people or property resulting from any ideas, methods, instructions or products referred to in the content.